An Integrated Filtering Antenna Array with High Selectivity and Harmonics Suppression

Chun-Xu Mao, Steven Gao, *Member*, *IEEE*, Yi Wang, *Senior Member*, *IEEE*, Zheng-Peng Wang, Fan Qin, Benito Sanz-Izquierdo, Qing-Xin Chu, *Senior Member, IEEE*

Abstract— In this paper, a new design of antenna array with integrated functions of filtering, harmonics suppression and radiation is proposed. The device employs a multi-port network of coupled resonators, which is synthesized and designed as a whole to fulfill the functions of filtering, power combination/division and radiation. The 50 Ω interfaces between the cascaded filter, power divider and antenna in traditional RF front-ends are eliminated to achieve a highly integrated and compact structure. A novel resonator-based four-way out-of-phase filtering power divider is proposed and designed. It is coupled to the patch array, rendering a fourth-order filtering response. The coupling matrix of the resonator network is synthesized. The physical implementations of the resonators and their couplings are detailed. Compared to a traditional patch array, the integrated filtering array shows an improved bandwidth and frequency selectivity. In addition, the harmonic of the antenna array is suppressed due to the use of different types of resonators. To verify the concept, a 2 × 2 filtering array at S band is designed, prototyped and tested. Good agreement between simulations and measurements has been achieved, demonstrating the integrated filtering antenna array has the merits of wide bandwidth, high frequency selectivity, harmonics suppression, stable antenna gain and high polarization purity.

Index Terms— Bandwidth, filtering antenna array, frequency selectivity, harmonics suppression, integrated design.

I. INTRODUCTION

The current developments of wireless systems such as mobile communications, wireless local area networks and satellite communications demand the RF front-end system to be compact, light weight, low cost and multi-functional. Traditionally, the different functional components in the front-end, such as the filter and antenna are designed separately and cascaded through 50 Ω terminals and matching networks. Due to the difference in bandwidths between the filter and the antenna, they are usually not well matched, especially at the edges of the operating band. This mismatch degrades the frequency performance of the system. Another critical issue in wireless communication systems is the interference caused by harmonics. These harmonics could be suppressed or eliminated in filter designs, for instance, by introducing transmission zeros [1], using spur-line filters [2] or discriminating coupling [3].

Microstrip antenna array has been widely used in wireless systems for its merits of low profile, light weight and low cost [4]. A large feeding network is often required to feed each antenna element with given magnitude and phase. Quarter wavelength transmission lines and matching stubs are commonly used for impedance matching. The feeding network could be very complex [5]. Due to the resonant characteristics and relatively high Q-values of microstrip antennas, microstrip arrays have the major drawback of narrow bandwidth. To enhance the bandwidth, techniques such as adding air gaps, increasing the thickness of the substrates have been used at the expense of increased thickness and complexity [5]-[7].

To overcome the aforementioned problems while maintaining a compact structure of the front end, the integrated design of filters, power dividers, antennas and other passive components is one promising solution. Much effort has been made into the research of passive component integration. In [8], novel multiplexers were demonstrated based on all-resonator structures, eliminating the conventional transmission-line based signal distribution networks. The integration of filters and antennas has attracted significant research interests during the past several years [9]-[22]. By virtue of their resonant nature, some antennas can serve as the last resonators of the filters. As a result, the antennas can contribute to the poles of the filter and therefore the bandwidth and frequency selectivity. In [9], a microstrip filtering antenna array was proposed by using coupled resonators to design the feeding network. To the best of our knowledge, [9] was the only filtering array previously demonstrated in the literature. Compared with [9], the filtering array in this paper achieves a much wider bandwidth (5.6% versus 3.0%) and a higher order filtering (4th order versus 3rd order) with a similar shape factor of a 2 × 2 array. In [17]-[18], the integrated design also helped suppress the harmonics in the high band of filtering antenna.

In this paper, a novel 2 × 2 antenna array using an all-resonator network is proposed. The filter and power dividing networks in traditional RF frontend are replaced by a group of coupled resonators. The array of patches serve not only as the radiating elements but also the last resonator of the filter. First, the network of resonators is represented by a coupling matrix and synthesized to guide the physical
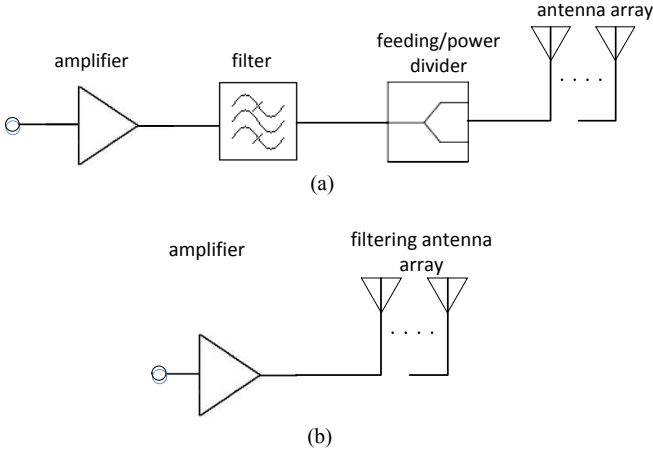
Fig.1. The architecture of a RF front-end with a power divider fed antenna array: (a) traditional, (b) proposed.

dimensioning of the circuits. Then, a resonator-based four-way out-of-phase power divider is designed. The divider is integrated with a patch array through coupling. Comparisons between the integrated filtering array and a traditional antenna array are made regarding the bandwidth, frequency selectivity and harmonics suppression. The harmonics of the integrated design is suppressed by the use of three types of resonators with different harmonics characteristics.

This paper is organized as follows. Section II explains the integration approach and the synthesis of the coupling matrix. Section III describes the design processes. Section IV presents the measured results followed by conclusion in Section V.

II. INTEGRATION APPROACH

A. RF front-end architecture

Fig. 1 (a) shows a traditional architecture of a RF front end with an antenna array fed by a power divider. The power divider and the antennas are designed individually with the assumption of ideal 50 Ω interfaces between them. However, this assumption is not always accurate, especially when the bandwidths of each component are different. In this case, the performance of the system will be deteriorated, especially around the edges of the operating band.

To overcome these problems, a compact, multi-functional and integrated architecture is proposed in this paper, as shown in Fig. 1(b). Here the filter, power-divider and antenna array are co-designed as a whole. As a result, the 50 Ω interfaces and the matching networks between them are removed. The overall bandwidth of the integrated system is no longer limited by the component with the narrowest band – the patch array in this case. Instead the bandwidth will be enhanced by coupling between the resonators and the resonant antennas.

B. Synthesis of the coupling matrix

The multiple functions - filtering, power division and radiation - are integrated into a single network of coupled resonators. It is essentially a four-way all-resonator based topology as proposed and shown in Fig. 2. The circles represent resonators or resonant antenna elements, whereas the lines
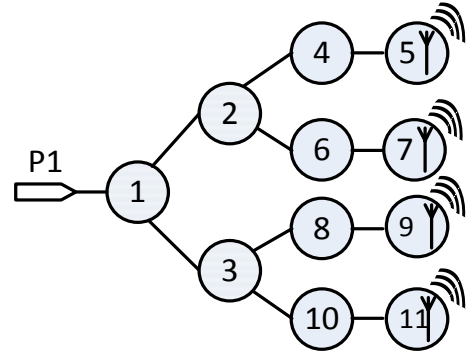

Fig. 2. The topology of coupled resonators for the fourth-order filtering array proposed in this paper.
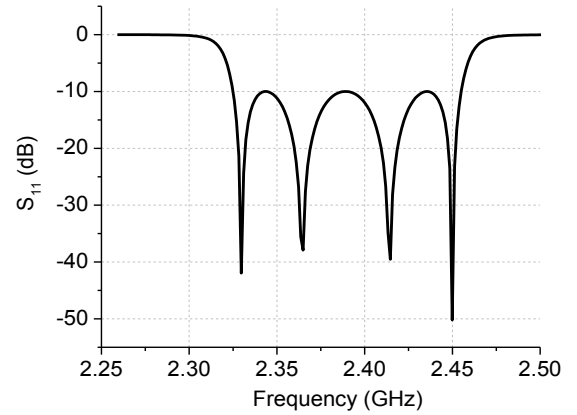

Fig. 3. Theoretical S-parameters of the proposed topology corresponding to the synthesized coupling matrix.

between them represent the coupling. It should be noted that the resonators 5, 7, 9 and 11 work as resonators and radiators simultaneously. The resonators 1, 2 and 3 act as the power distribution elements, which are traditionally realized by transmission-line T-junctions. Such a network has the fourth-order filtering characteristics. A single coupling matrix M can be used to represent the topology in Fig. 2. Due to its high symmetry, such a matrix can be directly synthesized. Detailed analyses can be found in [25]. Basically, the coupling coefficients M_{ij} of the multi-port network can be related to those of a fourth-order two-port Chebyshev filter, as denoted by M'_{ij}, using the following equations,

$$M_{12} = M'_{12}/\sqrt{2}, M_{24} = M'_{24}/\sqrt{2}, M_{45} = M'_{45}, M_{13} = M_{12},$$
$$M_{24} = M_{26} = M_{38} = M_{3,10}, M_{45} = M_{67} = M_{89} = M_{10,11}.$$

The specifications in this design are given as follows: Centre frequency $f_0 = 2.39$ GHz, bandwidth $BW = 130$ MHz, return loss $RL = 10$ dB, and order $N = 4$. The coupling coefficients and external quality factors can be derived as $Q_{ex} = 29.9$, $M_{12} = M_{13} = 0.0275$, $M_{24} = M_{26} = M_{38} = M_{3,10} = 0.0230$, $M_{45} = M_{67} = M_{89} = M_{10,11} = 0.0389$. $M_{i,j}$ is the coupling coefficient between the resonator i and j. All resonators are synchronously tuned, i.e. $M_{i,i} = 0$. It should be noted that no source-load coupling is considered in the synthesis. Fig. 3 shows the theoretical frequency response corresponding to the coupling matrix.
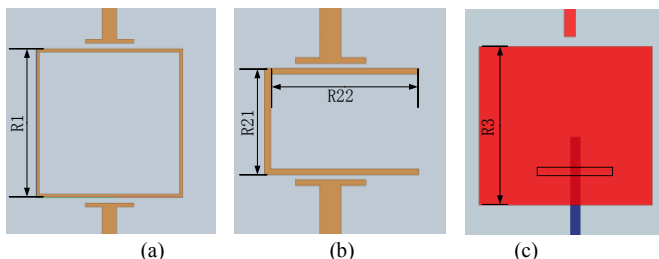
Fig. 4. Configuration of three types of resonators with weak coupling to the input and output ports: (a) ring strip resonator, (b) hairpin resonator and (c) square patch resonator. R1 = 23.6 mm, R21 = 12 mm, R22 = 17.5 mm, R3 = 31.5 mm.
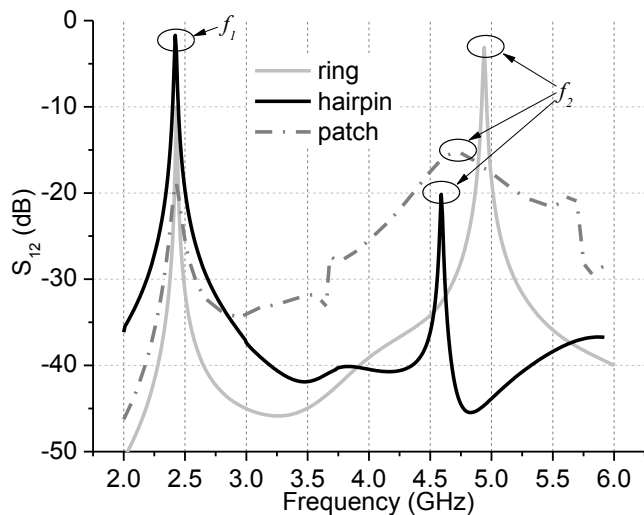

Fig. 5. The $|S_{21}|$ of the three resonators in Fig. 4.

III. DESIGN

A. Resonators and antennas

Microstrip resonators have been used to implement the topology in Fig. 2. Resonator 1, 2 and 3 should be symmetrical in geometry. The ring strip resonators are chosen due to their symmetry and high Q-value, as shown in Fig. 4(a). The total length of the resonator is about a wavelength at the resonant frequency. As for resonator 4, 6, 8 and 10, hairpin resonators, as shown in Fig. 4(b), are adopted to couple power to the ring strip resonator and to feed the antenna again through coupling in this design. The hairpin is a half-wavelength resonator. Resonators 5, 7, 9 and 11 are square patches, as shown in Fig. 4(c). They not only act as the radiating elements but also the last resonators of the filtering network. Therefore, they contribute to one pole in the frequency response. The length of the square patch is approximate a half of a guided wavelength. It is worth mentioning that here the patch antenna is treated as a two-port component as a first-order approximation to illustrate its resonance and harmonic performance. The different structures and therefore different resonant characteristics of the three types of resonators have the added benefit of having distinct harmonic frequencies. As shown in Fig. 5, when the fundamental modes of the resonators are tuned to the same frequency at 2.4 GHz, their second-order harmonics vary widely with each other. This property has been used to suppress
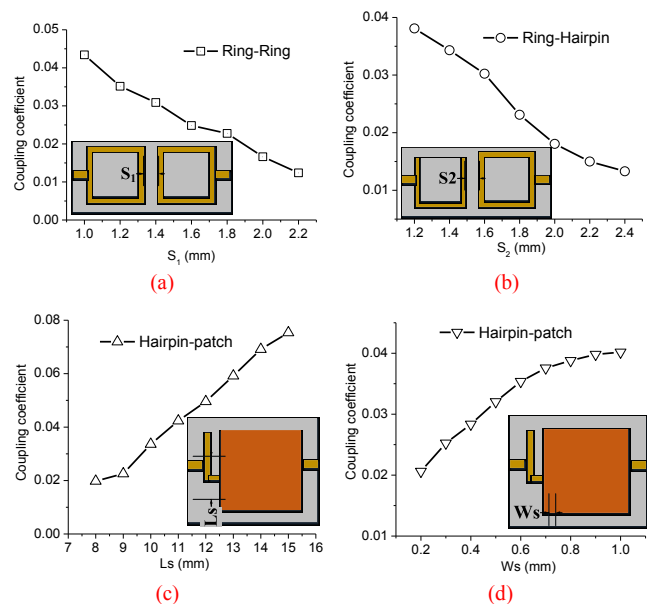

Fig. 6. Coupling coefficients between resonators: (a) two ring strip resonators with S_1 (b) ring strip resonator and hairpin resonator with S_2, (c) hairpin resonator and the patch resonator with length of slot Ls and (d) hairpin resonator and the patch resonator with width of slot Ws.

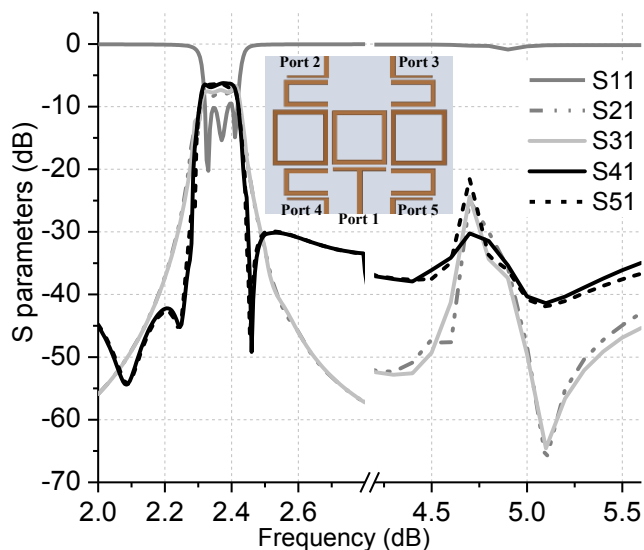the harmonics in the higher band.

B. Coupling

The couplings between the resonators are estimated using simulations. The coupling strength between the two ring resonators and between the ring resonator and hairpin resonator can be adjusted by changing the spaces (S_1, S_2) between them. The coupling between the hairpin and the patch can be realized through a slot in the ground and the coupling strength is controlled by tuning the length and width of the slot. All the coupling coefficients are extracted using (1) [23],

$$M_{ij} = \frac{f_j^2 - f_i^2}{f_j^2 + f_i^2} \tag{1}$$

where f_i and f_j are the resonant frequencies from the two coupled resonators. Using full-wave simulation, f_i and f_j can be obtained and coupling coefficients can be calculated.

Fig. 6 shows the coupling coefficients between the resonators as a function of geometry parameters. During these simulations, the couplings to the input and output ports are kept weak so as to ensure the revealed coupling characteristics are from the two interacting resonators. Fig. 6(a) shows the coupling between two ring strip resonators and Fig. 6(b) shows the coupling between the ring strip and the hairpin resonator. As for the coupling between hairpin resonator and patch resonator, which are located on different circuit layers, the coupling is realized by slitting a slot in the ground plane. By increasing the length or the width of the slot, the coupling coefficient increases, as presented in Fig. 6(c) and (d). To realize the required coupling coefficients, the initial values of the parameters have been found to be $S_1 = 1.5$ mm, $S_2 = 1.6$ mm, $L_S = 11$ mm and $W_S = 0.8$ mm.

(a)

Fig. 8. The simulated current distribution at 2.4 GHz.

(b)

Fig. 7. The simulated frequency response of the resonator-based four-way power divider: (a) magnitude, (b) phase.

Fig. 9. The |S41| (|S51|) with different *Dis*.

C. Resonator-based out-of-phase power divider

Without cascading with a separate filter, the resonator-based power divider demonstrates an embedded filtering function. Fig. 7(a) shows the circuit layout and the simulated S-parameter of the four-way third-order power divider. The power fed from the center ring strip resonator is divided and coupled to the other two ring resonators at both sides. This is then coupled to the hairpin resonator. The S-parameter in Fig. 7 shows a filtering performance with three poles in the band. These poles are introduced by the coupled resonators.

At the harmonic frequencies (4.5 to 5 GHz), the filtering divider detunes due to the different second-order harmonics among the different resonators. It is evident from Fig. 7(a) that the harmonics are suppressed as a result. It is also noted that as no decoupling structure (such as a resistor as in a Wilkinson divider) is used, the isolation between the four outputs is poor (-8 dB). However, this is not deemed as an issue in an antenna array design. In other cases when a graceful degradation is required in multi-channel devices such as multiport power
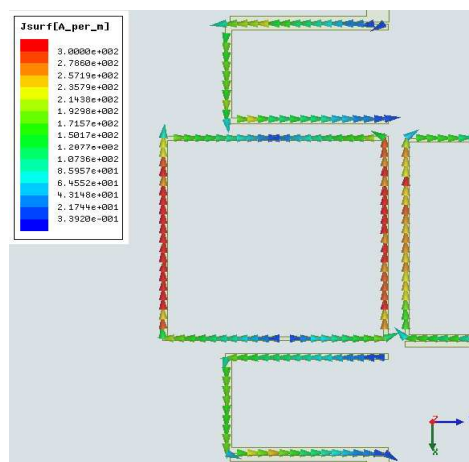
amplifiers, output isolation would be essential.

Fig. 7(b) shows the phase response of the power divider. Due to the symmetrical configuration, the port 2 and 3 have consistent phase response, so do the port 4 and 5. However, when we compare the port 2 and 4, or port 3 and 5, 180º phase difference can be observed. This can be visualized in the current density distribution at 2.4 GHz as presented in Fig. 8. The current reverses at the two coupling locations with the hairpin resonators. The electrical length between the two locations is about half of a wavelength, which causes the 180º phase difference. The out-of-phase output not only makes the design more compact, but also improves the cross polarization discrimination [24].

It is worth noting that the $|S_{41}|$ ($|S_{51}|$) response is different from the $|S_{21}|$ ($|S_{31}|$) response out of the band. For $|S_{41}|$ ($|S_{51}|$), three transmission zeros at 2.1, 2.25 and 2.45 GHz are visible, with the first two located at the lower band and the third one located at the higher band. These transmission zeros can be attributed to the source-load coupling between the port 1 and Port 4 (5) which are on the same side of the circuit and in proximity, as well as the cross coupling between the non-adjacent ring and the hairpin. These couplings were not
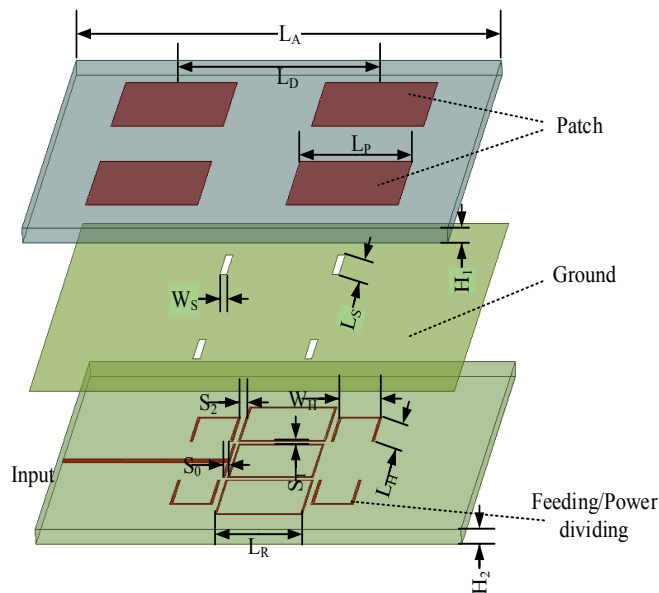
Fig. 10. Exploded view of 2 × 2 filtering antenna array. L_A = 120 mm, L_P = 31.5 mm, L_D = 60 mm, Ls= 11.6 mm, W_S = 0.9 mm, L_R = 24.6 mm, L_H = 16.7 mm, W_H =12 mm, S_0 = 0.25 mm, S_1 = 1.7 mm, S_2 = 1.6 mm, H_1 = 1.525 mm, H_2 = 0.787 mm.

considered in the synthesis of the coupling matrix. However, the resultant transmission zeros significantly improve the frequency selectivity of the filtering divider. Parameter studies have been performed to investigate the relationship between the couplings and the transmission zeros. As shown in Fig. 9, the coupling between the source (Port-1) and load (Port-4 and 5) is varied by tuning the distance *Dis* between the hairpin and the feedline at Port-1. This should also affect the cross coupling between the non-adjacent ring and the hairpin. When *Dis* is over 10 mm, only one transmission zero is observable at the lower band and the other at the higher band. When *Dis* decreases, two transmission zeros appear at the lower band, whereas the third one shifts closer to the pass-band. This mechanism of creating and controlling the transmission zero can be used to design filter-antennas with further improved frequency selectivity without increasing the order of the filters. As an attempt to further verify the origin of the transmission zeros, an optimisation-based method has been used to extract the coupling matrix that reproduces the transmission zeros. It has been found that a weak source-load coupling and cross-coupling can indeed result in three zeros. The positions of the first two zeros but not the third one can be accounted for. The transmission zero in the upper stop band may be affected by stray couplings that are not yet fully apprehended.

D. Filtering antenna array

Based on the topology in Fig. 2 and replacing the outputs of the third-order filtering power divider with the radiating patches, an antenna array with integrated fourth-order filtering characteristics can be realized. Fig. 10 is the exploded view of the multi-layer structure of the 2 × 2 filtering antenna array. The radiating patches are printed on the top layer of the upper substrate (Rogers 4003 with a dielectric constant of 3.55). The filtering power dividing network is printed on the bottom layer

of the lower substrate (Rogers 5880 with a dielectric constant of 2.2). The power dividing network and the patches share a common ground plane in the middle layer. The patches on the top layer act as the last resonators and coupled to the hairpin resonators through the slots in the ground plane. The space between the patches L_D is 60 mm, i.e. 0.48 λ at the center frequency of 2.39 GHz. It should be noted that in this all-resonator based design the traditionally separated filter and
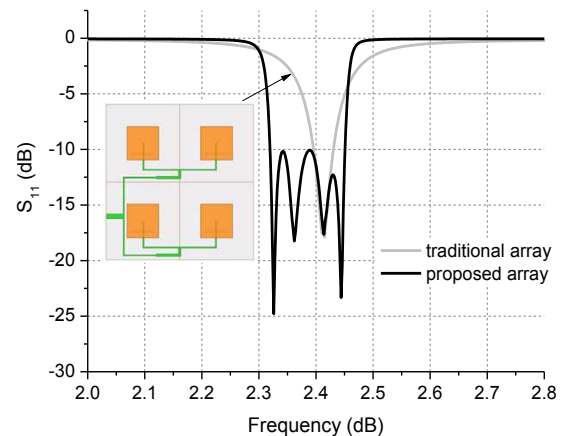

Fig. 11. The simulated |S₁₁| of the filtering antenna array and a traditional antenna array.

Fig. 12. The simulated |S₁₁| and antenna gain of the filtering antenna array in comparison with a traditional patch array over an extended frequency range including the harmonics.

the interfaces between the filter and antenna are eliminated, which results in a compact and highly integrated structure. The design and simulation were performed using High Frequency Simulation Software (HFSS 15), and the optimized parameters are given in the caption of Fig. 10.

E. Comparison with traditional design

Fig. 11 shows the simulated S₁₁ of the filtering antenna array in comparison with a traditional patch array. The patches of the traditional patch array are fed by a microstrip-line power divider through the slots in the ground and the other parameters of the two patch array are identical. It can be seen from Fig. 11 that four reflection zeros at 2.33, 2.36, 2.41 and 2.45 GHz are clearly visible for the integrated antenna array demonstrating the expected fourth-order filter characteristics. A -10 dB

impedance bandwidth of 5.6% is achieved. In contrast, only one resonant mode can be observed for the traditional patch array and the fractional bandwidth is 1.6%. The integrated design improves the bandwidth of the antenna array significantly. It should also be noted that the frequency selectivity of the proposed antenna is significantly improved due to the higher order resonant characteristics. To better quantify the frequency selectivity, the ratio of the -10 dB

TABLE I
PARAMETER COMPARISON WITH TRADITIONAL ARRAY

Antenna Type	Traditional Array	Proposed Array
Number of Resonant Poles	1	4
Fractional Bandwidth	1.60%	5.60%
Frequency Selectivity (BW$_{-10dB}$/BW$_{-3dB}$)	30%	87%
Harmonic Level ($|S_{11}|$)	-6 dB	-0.7 dB
Gain (In band)	9.9 dBi	9.7 dBi
Gain (Harmonic)	10.1 dBi	-15 dBi

(a)   (b)

Fig. 13. Photograph of the 2×2 filtering antenna array: (a) front view, (b) back view.

bandwidth (BW$_{-10dB}$) and the -3 dB bandwidth (BW$_{-3dB}$) is estimated. From Fig. 11, the ratios for the traditional antenna array and the integrated antenna array are calculated as 30% and 87%, respectively.

Higher order harmonics are common in distributed microwave components such as microstrip filters and antennas. This is a source of interference and could degrade the quality of the system. In this integrated design, the use of three types of resonators with different harmonics as discussed in Section III (Fig. 4 and 5), suppresses the harmonics effectively. This is evident in Fig. 12 which show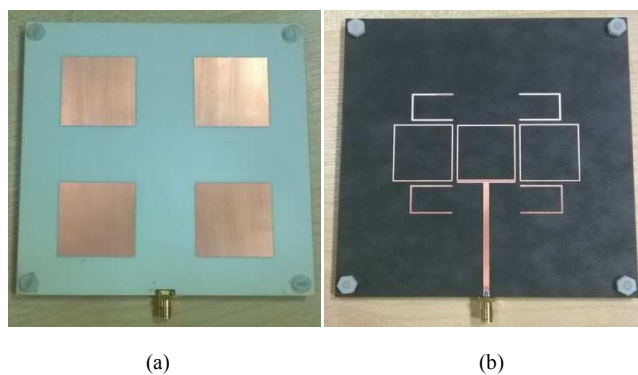s the simulated S$_{11}$ and realized gains of the proposed filtering antenna array and the traditional patch antenna array over a wide frequency range. For the traditional antenna, a spurious band occurs around 4.5 GHz with a return loss of 6.2 dB due to harmonics. For the proposed antenna array, the harmonic band is almost eliminated with a return loss of only 0.7 dB. From the gain curves, the gain reaches 10.1 dBi at the harmonics for the traditional array. This is suppressed by 25 dB in the proposed design. In the fundamental operation band, the traditional array has a peak gain of 9.9 dBi at 2.4 GHz, and slowly decreases. The integrated design has a flat gain of 9.7 dBi between 2.30 and 2.42 GHz. It drops sharply to below -20 dBi below 2.24 GHz and above 2.53 GHz. Table I summaries the parameter

comparison with the traditional antenna in terms of the resonant poles, bandwidth, frequency selectivity, harmonic level and gain in band as well as gain at the harmonic.

IV. RESULTS AND DISCUSSIONS

Fig. 13 shows the prototype of the 2 × 2 filtering antenna array. The antenna is measured using a ZVL vector network
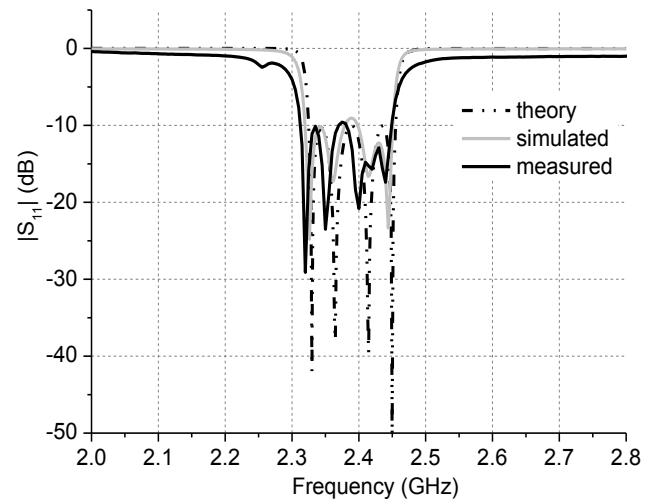

Fig. 14. The theoretical, simulated and measured $|S_{11}|$ of the filtering antenna array.

analyzer. The simulated and measured S$_{11}$ as well as the theoretical result from the synthesis are presented in Fig. 14. The measured result agrees very well with the simulated and theoretical results with an impedance bandwidth from 2.31 GHz to 2.46 GHz. There is an unexpected dip between 2.2 and 2.3 GHz. The cause of this is unclear. It may be a result of spurious coupling.

Fig. 15 shows the normalized simulated and measured radiation patterns of the filtering antenna array in E and H plane for co- and cross-polarization. The patterns exhibit expected radiation performance with maximum antenna gain in the broadside. The cross polarization discrimination (XPD) in the E and H plane are better than -36 dB and -28 dB, respectively, which is attributed to the slot coupling and the out-of-phase power divider. Another feature of this design is that, different from [9], the feeding network is shielded from the array.

Fig. 16 shows the measured and simulated realized antenna gains of the filtering antenna array over a wide frequency range from 2 to 5.4 GHz. The simulated gain of the traditional antenna array is also included for comparison. It is observed that the simulated and measured results agree well with each other. The filtering antenna array has a flat gain response of 9 dBi from 2.30 to 2.45 GHz. In the measured gain-frequency curve, two nulls can be observed at the both sides of the pass-band, resulting in a rapid drop of the gain out of the band. The gain reduces to -25 dBi below 2.24 GHz and above 2.53 GHz. These nulls can be attributed to the source-load coupling and the cross coupling as discussed in Section III-C. It is worth noting that the frequencies of the nulls in the gain curve are slightly different from those of the transmission zeros of the power divider in Fig. 9. This is because in the filtering array the

hairpins are coupled to the patch antennas rather than the output ports as in the power divider. The characteristics of the couplings have changed. Nevertheless the nulls still make a significant impact on the increase of the frequency selectivity.

Around the frequency bands of harmonic frequencies, the antenna gains are significantly reduced by 22 dB as compared with the traditional patch antenna. This verifies the capability of harmonic suppression of the integrated design. There are

(a)

(b)

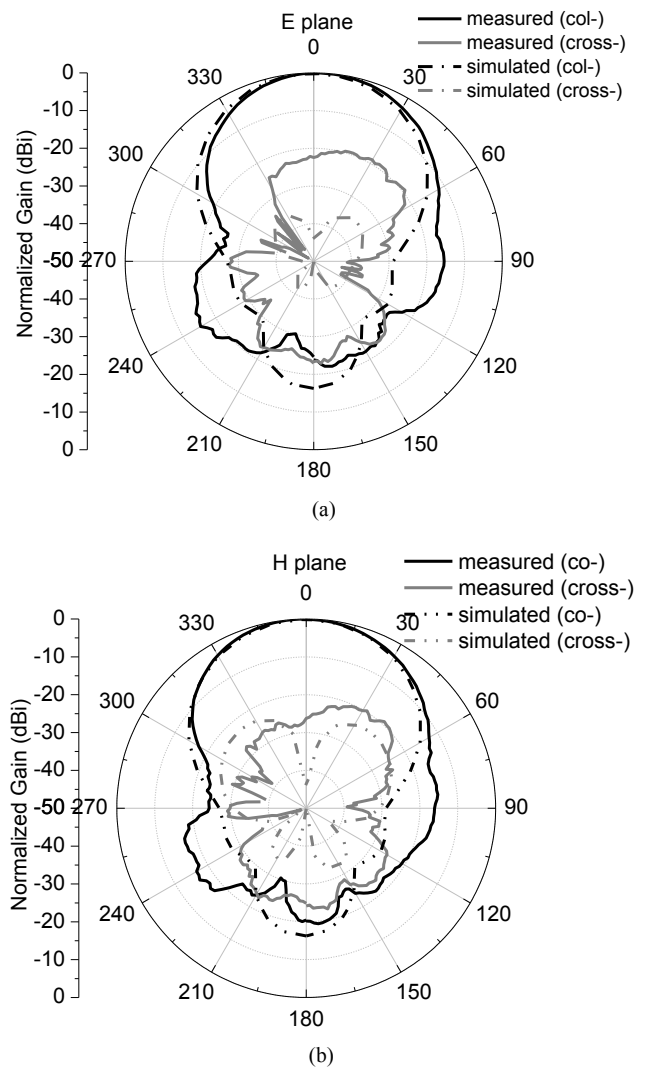Fig. 15. The normalized measured co- and cross-polarization radiation patterns at 2.4 GHz: (a) E plane, (b) H plane.
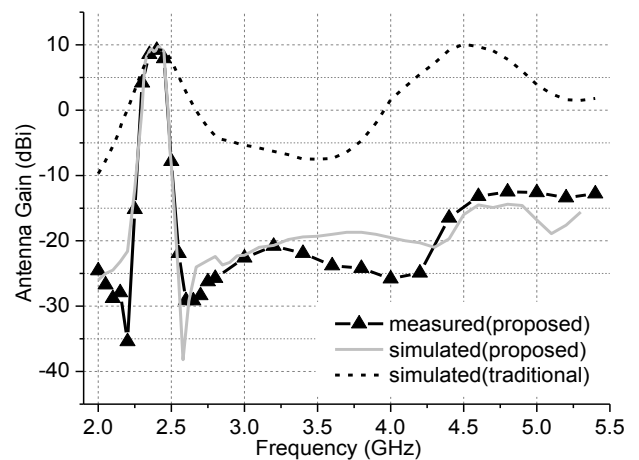

Fig. 16. The measured gain of the filtering antenna array as a function of frequency.

some small discrepancies between the simulated and the measured gain curves especially outside the operation band. This is due to the reduced measurement sensitivity at these rejection bands where the power level is very low.

TABLE II

COMPARISON WITH OTHER FILTERING ANTENNAS

Antennas	[9]	[21]	This work
FBW	3.0%	6.2%	5.6%
Antenna Size	1.06 λ×1.06 λ	0.86 λ×1.16 λ	0.96 λ×0.96 λ
In-band Gain	9.6 dBi	6.1 dBi	9.7 dBi
Number of Substrates Used	1	1	2
Gain at Harmonic	-	-5 dBi	-15 dBi

For the traditional antenna array, the gain decreases slowly when the frequency deviates from the center frequency. The comparison of the gains between the two antenna arrays demonstrates that the integrated filtering antenna array has a much improved performance of frequency selectivity and harmonic suppression.

Table II compares the filtering antenna in this paper with the only other reported filtering array in the literature [9] and one filtering antenna in [21]. The comparison mainly focuses on bandwidth, antenna size, gain, number of substrates and gain at the harmonic. This comparison shows that this work exhibits a wider bandwidth than that in [9] and an improved harmonic suppression than that in [21]. These enhancements are attributed to the mixed use of different types of resonators and the out-of-phase divider. A disadvantage is the use of two substrates.

V. CONCLUSION

In this paper, a 2 × 2 highly integrated antenna array with high frequency selectivity and improved bandwidth has been proposed and demonstrated. First, the topology of the filtering antenna is studied and the coupling matrix is synthesized to guide the design process. Then, the resonant characteristics of the three types of resonators are investigated and an all-resonator-based third-order four-way out-of-phase power divider is designed. The couplings between the resonators are studied. The integrated antenna array shows an improved bandwidth and frequency selectivity when compared with the traditional antenna array. Furthermore, harmonics are suppressed by utilizing different types of resonators. The measured results agree very well with the simulations, showing that the proposed filtering antenna array has excellent performance in terms of frequency selectivity, bandwidth, radiation characteristics and antenna gain.

It is also observed that the source-load coupling and cross coupling between non-adjacent resonator are existing in the proposed design, which were not fully considered in the initial synthesis of the coupling matrix, have helped generate transmission zeros in the power divider and then nulls in the gain curve. These useful features further increase the frequency selectivity of the filtering array. Parameter studies have showed potential ways to control the transmission zeros. In the future, a more systematic approach can be taken to make use of the coupling and implement transmission zeros for the benefit of the integrated design of filters and antennas.

REFERENCES

[1] S. Sun and L. Zhu, "Periodically Nonuniform Coupled Microstrip-Line Filters With Harmonic Suppression Using Transmission Zero Reallocation," *IEEE Trans. Microw. Theory Techn., vol.* 53, no. 5, pp. 1817-1822, May 2005.

[2] A. Griol, J. Marti and L. Sempere, "Microstrip Multistage Coupled Ring Bandpass Filters Using Spur-Line Filters for Harmonic Suppression," *Electron. Lett.*, vol. 37, no. 9, pp. 572-573, Apr. 2001.

[3] X. Y. Zhang, Q. Xue, "Harmonic-Suppressed Bandpass Filter Based on Discriminating Coupling," *IEEE Microw. Wireless Compon. Lett.*, vol. 19, no. 11, pp. 695-697, Nov. 2009.

[4] S. Gao, Q. Luo and F. Zhu, Circularly Polarized Antennas, *IEEE Press & Wiley*, Feb. 2014, UK.

[5] D. Pozar and S. Targonski, "A shared-Aperture Dual-Band Dual-Polarized Microstrip array," *IEEE Trans. Antennas and Propag.,* vol. 49, no. 2, pp. 150-157, Feb. 2001.

[6] S. Gao and A. Sambell, "Low-Cost Dual-Polarized Printed Array with Broad Bandwidth," *IEEE Trans. Antennas Propag.*, vol. 52, no. 12, pp. 3394-3397, Dec. 2004.

[7] S. Gao and A. Sambell, "Dual-Polarized Broad-Band Microstrip Antenna Fed by Proximity Coupling," *IEEE Trans. Antennas Propag.*, vol. 53, no. 1, pp. 526-530, Jan. 2005.

[8] X. B. Shang, Y. Wang, W. L. Xia and M. Lancaster, "Novel Multiplexer Topologies Based on All-Resonator Structure," *IEEE Trans. Microw. Theory Techn.*, vol. 61, no. 11, pp. 3838-3845, Nov. 2013.

[9] C. K. Lin and S. J. Chung, "A Filtering Microstrip Antenna Array," *IEEE Trans. Microw. Theory Techn., vol.* 59, no. 11, pp. 2856-2863, Mar. 2011.

[10] F. Queudet, I. Pele, B. Froppier, Y. Mahe, and S. Toutain, "Integration of Pass-Band Filters in Patch Antennas," in *Proc. 32nd Eur. Microw. Conf.,* 2002, pp. 685–688.

[11] A. Abbaspour-Tamijani, J. Rizk, and G. Rebeiz, " Integration of filters and microstrip antennas," in *Proc. IEEE AP-S Int. Symp.,* Jun. 2002,pp. 874–877.

[12] T. L. Nadan, J. P. Coupez, S. Toutain, and C. Person, "Optimization and miniaturization of a filter/antenna multi-function module using a composite ceramic-foam substrate," in *IEEE MTT-S Int. Microw. Symp. Dig.,* Jun. 1999, pp. 219–222.

[13] C. K. Lin and S. J. Chung, "A Compact Filtering Microstrip Antenna with Quasi-Elliptic Broadside Antenna Gain Response" *Antenna Wireless Propag. Lett.,* vol. 10, pp. 381–384, 2011.

[14] X. W. Chen, F. X. Zhao, L. Y. Yan and W. M. Zhang, "Compact Filtering Antenna With Flat Gain Response Within the Passband," *Antenna Wireless Propag. Lett.,* vol. 12, pp. 857–860, 2013.

[15] O. A Nova, J. C Bohorquez, N. M Pena, G. E Bridges, L. Shafai and C. Shafai, "Filter-Antenna Module Using Substrate Integrated Waveguide Cavities," *Antenna Wireless Propag. Lett.*, vol. 10, pp. 59–62, 2011.

[16] W. J. Wu, Y. Z. Yin, S. L. Zuo, Z. Y. Zhang and J. J. Xie, "A New Compact Filter-Antenna for Modern Wireless Communication Systems," *Antenna Wireless Propag. Lett.*, vol. 10, 2011, pp. 1131–1134.

[17] L. Yang, P. Cheong, L. Han, W. W. Choi, K. W. Tam and K. Wu, "Miniaturized Parallel Coupled-Line Filter-Antenna With Spurious Response Suppression," *Antenna Wireless Propag. Lett.,* vol. 10, pp. 726–729, 2011.

[18] D. Zayniyev and D. Budimir, "An Integrated Antenna-Filter with Harmonic Rejection," *3rd European Conf. on Antennas and Propag.,* 2009, pp. 393-394.

[19] C. T. Chuang and S. J. Chung, "Synthesis and Design of a New Printed Filtering Antenna," *IEEE Trans. Antennas and Propag.,* vol. 59, no. 3, pp. 1036-1042, Mar. 2011.

[20] J. H. Zuo, X. W. Chen, G. R. Han, L. Li and W. M. Zhang, "An Integrated Approach to RF Antenna-Filter Co-Design," *Antenna Wireless Propag. Lett.,* vol. 8, pp. 141–144, 2009.

[21] Y. Yusuf and X. Gong, "Compact Low-Loss Integration of High-Q 3-D Filters with Highly Efficient Antennas," *IEEE Trans. Microw. Theory Techn.,* vol. 59, no. 4, pp. 857-865, Apr. 2011.

[22] Y. Yusuf and X. Gong, "Co-Designed Substrate-Integrated Waveguide Filters With Patch Antennas," *IET Antennas, Propag.,* vol. 7, no. 7, pp. 493-501, Apr. 2013.

[23] J. S. Hong and M. J. Lancaster, *Microwave Filger for RF/Microwave Application*. New York: Wiley, 2001.

[24] J. Granholm and K. Woelders, "Dual Polarization Stacked Microstrip Patch Antenna Array With Very Low Cross-Polarization," *IEEE Trans. Antennas and Propag.,* vol. 49, no. 10, pp. 1393-1402, Oct. 2001.

[25] A. Mohammed, Y. Wang, "Four-way Waveguide Power Dividers with Integrated Filtering Function", in the *44th European Microwave Conference*, Paris, France, Sept. 2015.